Phonon calculations in cubic and tetragonal phases of SrTiO₃: A comparative LCAO and plane-wave study

Robert A. Evarestov,[1] Evgeny Blokhin,[2] Denis Gryaznov,[2,3] Eugene A. Kotomin,[2,3] and Joachim Maier[2]

[1]*Department of Quantum Chemistry, St. Petersburg State University, Peterhof, Russia*
[2]*Max-Planck Institute for Solid State Research, Stuttgart, Germany*
[3]*Institute for Solid State Physics, University of Latvia, Riga, Latvia*

The atomic, electronic structure and phonon frequencies have been calculated in cubic and low-temperature tetragonal SrTiO₃ phases at the *ab initio* level. We demonstrate that the use of the hybrid exchange-correlation PBE0 functional gives the best agreement with experimental data. The results for the standard generalized gradient approximation (PBE) and hybrid PBE0 functionals are compared for the two types of approaches: a linear combination of atomic orbitals (CRYSTAL09 computer code) and plane waves (VASP5.2 code). The relation between cubic and tetragonal phases and the relevant antiferrodistortive phase transition is discussed in terms of group theory and is illustrated with analysis of calculated soft-mode frequencies at the Γ and R points in the Brillouin zone. Based on phonon calculations, the temperature dependence of the heat capacity is in good agreement with experiment.

I. INTRODUCTION

ABO₃-type perovskites continue to attract great attention due to fundamental problems of materials, physics, and chemistry and also numerous high technological applications.[1,2] In particular, one of the best-studied perovskites is SrTiO₃ (hereafter, referred to as STO), which serves as a prototype for a wide class of perovskites.[3] This incipient ferroelectric reveals the antiferrodistortive (AFD) phase transition near 105 K.[4] It was shown that the soft phonon mode at the R point of the Brillouin zone (BZ) of cubic crystal is condensed below 105 K resulting in tetragonal lattice distortion with a slight unit-cell stretching (see Refs. 5 and 6 and references therein) and a TiO₆ octahedra antiphase rotation in the nearest unit cells along the c axis. Additional interest in STO at 90s was fueled by a suggestion about possible ferroelectric transition around 37 K (Ref. 7) (see discussion of this hypothesis in Refs. 8 and 9).

Despite STO revealing anomalous dielectric properties at low temperatures, it remains a paraelectric down to 0 K, due to both above-mentioned AFD phase transition and quantum effects.[10] For this reason, STO is also called a *quantum paraelectric*.

First *ab initio* calculations on STO electronic structure and phonon frequencies were started in 90s (see Refs. 5 and 11 and references therein). Since tetragonal structure transformation is very small, STO is a perfect model system for testing accuracy and predicting ability of new theoretical methods. Two main techniques for phonon calculations are the *direct frozen-phonon* (DFP)[12] and the *linear-response* (LR)[13] methods, both being completely independent of any experimental data and fitted parameters. The literature analysis of the applications of these methods to a cubic STO reveals rather inconsistent results concerning the presence of the soft modes at the different BZ points (and, if present, whether the corresponding frequencies are real or imaginary).

In particular, the calculations by Sai and Vanderbilt[5] based on the density functional theory (DFT) in the local-density approximation (LDA) combined with plane waves (PWs) within the DFP method have shown the concurrent character of

AFD and ferroelectric instabilities, i.e., hardening of the AFD R phonon and softening of the ferroelectric Γ phonon with the volume increase with respect to theoretical equilibrium. A series of calculations performed by Wahl *et al.*,[14] using the PW formalism within the DFP method as implemented in the VASP code [LDA, generalized gradient approximation (GGA), PBE, and hybrid Hartree-Fock (HF)-DFT Heyd-Scuseria-Ernzerhof (HSE) functionals] revealed the soft mode at the Γ point being real for LDA and imaginary for the PBE and HSE methods. LaSota *et al.*[11] and Lebedev,[15] in the linear augmented PW-LDA calculations within the LR method, obtained imaginary soft modes at the M, R, and Γ points of the BZ. Moreover, other calculations on the lattice dynamics of the cubic STO could be mentioned.[16–19]

Concerning the AFD phase, there is only the PW-LDA study[5] dealing with phonons. However, the AFD phase geometry obtained in this paper is quite far from experiment. In fact, there is the only hybrid B3PW study[20] within the linear combination of atomic orbitals (LCAO) formalism where the correct geometry of the AFD phase and its energetic preference with respect to the cubic phase was predicted. It was shown therein that the doubling of the unit cell, despite tiny tetragonal distortion, changes the indirect band gap for a direct one, which is well observed in photoconductivity studies. Understanding of the relation between observed AFD phase transition and phonon symmetry (e.g., which modes are expected to soften) needs a careful group-theoretical analysis, which is performed in this paper. Such analysis is also important for the classification of calculated phonon frequencies (Raman, infrared, or silent) and comparison with experimental frequencies (e.g., neutron-scattering measurements suggest phonon symmetry). Note also that a traditional factor-group analysis used in the literature could be applied only to the Γ-point phonons.

We performed this study using two approaches (LCAO and PW) and DFT functionals (GGA-type PBE, as well as hybrid PBE0 and B3PW) in order to understand their corresponding roles in a description of the atomic, electronic, and vibrational properties of the cubic and AFD phases of STO. Furthermore, this paper also has been stimulated by the deficiency in

first-principles studies of the heat capacity and phonons in the STO tetragonal phase.

This paper is organized in the following way. In Sec. II, the group-theoretical analysis of the cubic and AFD phases and relevant phase transformation in STO is performed. The computational details are discussed in Sec. III. The main results for atomic and electronic structures and phonon frequencies obtained for cubic and AFD phases are summarized in Sec. IV along with the calculations of the heat capacities and the Helmholtz free energies. Lastly, the conclusions are summarized in Sec. V.

II. PHONON SYMMETRY IN CUBIC AND TETRAGONAL PHASES

The STO cubic phase (space group (SG) $Pm\bar{3}m$--O_h^1) represents an example of the ideal perovskite-type cubic ABO_3 structure. We set the octahedrally coordinated B cation at the Wyckoff position $1a$ $(0,0,0)$, the A cation at $1b$ $(1/2,1/2,1/2)$, and the anion O at $3d$ $(1/2,0,0)$ [Table I and Fig. 1(a)]. To analyze the symmetry of phonon states, the method of induced representations (hereafter, reps) of space groups can be used.[21,22] The total dimension n of the induced rep (called the mechanical rep) equals $3N$ (N is the number of atoms in the primitive cell and equals 5 for the ideal perovskite).

TABLE I. Wyckoff positions and phonon symmetry in cubic and tetragonal AFD SrTiO$_3$.

$Pm\bar{3}m$ O_h^1 (SG 221)			$I4/mcm$ D_{4h}^{18} (SG 140)	
	Γ	R		Γ
Ti			Ti	
$1a$ $(0,0,0)$			$2c$ $(0,0,0)$	
O_h, t_{1u} (x,y,z)	4^- (t_{1u})	4^-	C_{4h} a_u (z)	a_{1u} a_{2u}
			e'_u (x,y), $e''_u(x,y)$	$2e_u$
				$t_{1u} \to a_{2u}\, e_u$
Sr			Sr	
$1b$ $(0.5,0.5,0.5)$			$2b$ $(0,0.5,0.25)$	
O_h, t_{1u} (x,y,z)	4^- (t_{1u})	5^+	D_{2d} b_2 (z)	a_{2u} b_{2g}
				$R_{5+} \to b_{2g}\, e_g$
			e (x,y)	e_g e_u
				$t_{1u} \to a_{2u}\, e_u$
O			O	
$3d$ $(0.5,0,0)$			$2a$ $(0,0,0.25)$	
D_{4h}, a_{2u} (z)	4^- (t_{1u})	1^+3^+	D_4 a_2 (z)	a_{2g} a_{2u}
e_u (x,y)	4^- (t_{1u})	4^+5^+	e (x,y)	e_g e_u
	5^- (t_{2u})			
				$R_{1+} \to a_{2g}$
				$R_{3+} \to e_g$
				$t_{1u} \to a_{2u}\, e_u$
			O	
			$4h$ $(-u+0.5,u,0)$	
			C_{2v} a_1 (z)	a_{1g} b_{2g} e_u
			b_1 (x)	b_{1g} a_{2g} e_u
			b_2 (y)	a_{2u} b_{1u} e_g
				$R_{4+} \to b_{1g}\, e_g$
				$R_{5+} \to b_{2g}\, e_g$
				$t_{1u} \to a_{2u}\, e_u$
				$t_{2u} \to b_{1u}\, e_u$

SG 221: $Pm3m$, $T_{\mathrm{exp.}} > 105$ K
$a_0 = 3.905$ Å

SG 140: $I4/mcm$, $T_{\mathrm{exp.}} < 105$ K
$\sqrt{2}a_0 \approx a = 5.507$ Å, $2a_0 \approx c = 7.796$ Å
oxygen distortion in $8h$, $u=0.241$
vertical cell stretching, $c/(\sqrt{2}a)=1.001$

Sr 0.5 0.5 0.5 ($1b$)	Sr 0.00 0.50 0.25 ($4b$)
Ti 0.0 0.0 0.0 ($1a$)	Ti 0.00 0.00 0.00 ($4c$)
O 0.5 0.0 0.0 ($3d$)	O 0.00 0.00 0.25 ($4a$)
	O u $u+0.50$ 0.00 ($8h$)
(a)	(b)
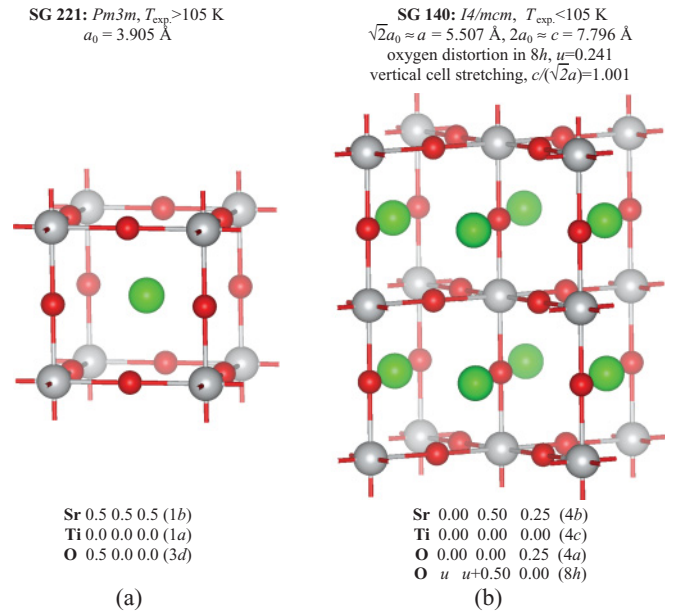
FIG. 1. (Color) Cubic (a) and tetragonal AFD (b) STO. (Green balls) Sr atoms, (gray balls) Ti, and (red balls) O atoms.

Table I shows the phonon symmetry in the STO crystal for Γ $(0,0,0)$ and R $(1/2,1/2,1/2)$ symmetry points of the BZ for a simple cubic lattice. The space group O_h^1 irreducible representations (irreps) are labeled according to Ref. 23. The space group irreps are induced from those site symmetry group irreps, which correspond to transformations of the atomic displacements (x,y,z): t_{1u} of the site symmetry group O_h (Ti and Sr atoms); a_{2u}, e_u of the site symmetry group D_{4h} (O atom).

One can obtain four t_{1u} modes and one t_{2u} mode at the Γ point of the BZ (one t_{1u} mode is acoustic). Three phonon modes of the t_{1u} symmetry are infrared active, and one mode of the t_{2u} symmetry is neither infrared nor Raman active (silent mode). The latter mode is connected with the displacements of O atoms only. Three modes 1^+, 3^+, and 4^+ at the R point of the BZ (with the degeneracy 1, 2, and 3, respectively) are displacement modes of the O atom only. The threefold degenerated R_{4-} and R_{5+} modes are Ti and Sr-O modes, respectively.

The second-order structural phase transition at 105 K reduces the symmetry from cubic (O_h^1) to tetragonal (space group $I4/mcm$-D_{4h}^{18}). The primitive unit cell of the body-centered tetragonal lattice consists of ten atoms (the cubic unit cell is doubled). Figure 1(b) shows the crystallographic (quadruple) unit cell of the body-centered tetragonal lattice and the occupations of Wyckoff positions by atoms. It is seen that O atoms are separated in two nonequivalent orbits: $4a$ (two atoms) and $8h$ (four atoms). The quadruple unit-cell parameters in the undistorted pseudocubic structure are $a = b = a_0\sqrt{2}$, $c = 2a_0$, where a_0 is the lattice constant of the cubic phase. The structural parameter $u = 0.25$ defines the oxygen $8h$ position in the undistorted pseudocubic structure. Thus, the experimental cubic lattice parameter $a_0 = 3.905$ Å (at room temperature) gives the undistorted pseudocubic structure with $a = b = 5.522$ Å, $c = 2a_0 = 7.810$ Å, which are close to the experimental $a = 5.507$ Å, $c = 7.796$ Å (Ref. 24) for a real distorted tetragonal structure. The experimental value $u = 0.241$ (Ref. 25) is close to

$u = 0.25$ for the undistorted pseudocubic structure. Thereby, the cubic-to-tetragonal phase transition can be considered as the tetragonal supercell generation with the transformation matrix $\begin{pmatrix} 1 & 1 & 0 \\ -1 & 1 & 0 \\ 0 & 0 & 2 \end{pmatrix}$ and the further small structural distortion.

The BO_6 octahedra distortions are considered often in terms of tilting (see Ref. 26 and references therein). By this, one means the tilting around one or more of the BO_6 symmetry axes allowing greater flexibility in the coordination of the A cation while leaving the environment of the B cation essentially unchanged. The tilt of one octahedron around one of these axes determines (via the corner connections) the tilts of all the octahedra in the plane perpendicular to this axis. The successive octahedra along the axis can be tilted in either the same or the opposite sense (in-phase and out-of-phase tilts). The group-theoretical analysis of octahedral tilting is described in detail in Ref. 26 where the irrep associated with the out-of-phase tilts, R_{4+}, is shown.

The symmetry of phonons in the AFD STO phase at the Γ point of the BZ is shown in Table I along with the splitting of the phonon frequencies due to lowering of the symmetry. The symmetry of acoustic phonons is $(a_{2u} + e_u)$; eight modes are infrared active $(3a_{2u} + 5e_u)$; seven modes are Raman active $(a_{1g}, b_{1g}, 2b_{2g}, 3e_g)$. The silent modes have the symmetry a_{1u}, b_{1u}, and twice a_{2g}.

As seen from Table I, a_{1g} and b_{1g} Raman active phonons arise due to the displacements of the O atoms only. The Raman active modes with the symmetry b_{2g} and e_g are Sr-O vibrational modes. The vibrations connected with Ti-atom displacements are active only in infrared spectra (a_{2u}, $5e_u$ phonons). The relation between the active vibrational modes with the displacements of concrete atoms makes the interpretation of the experimental infrared and Raman spectra easier (see Sec. IV).

The calculations of phonon frequencies in a cubic high-temperature phase (presented below) clearly demonstrates that the soft phonon mode symmetry is R_{4+} and, in this way, confirms the results of the group-theoretical analysis. In Secs. III–V, we discuss the computational details of the present phonon calculations and compare them with those found in the experimental and other theoretical studies.

III. CALCULATION DETAILS

In this paper, the DFP method was chosen for phonon calculations as it can, unlike the LR method, be used in conjunction with any external atomistic simulation code (ability to compute forces is only required). To obtain the phonon frequencies and thermodynamic functions within the DFP method, three steps are required:[27] (1) structure optimization, (2) construction of a supercell based on optimized structure and displacing atoms inside it, and (3) calculation of induced forces and the corresponding force matrix diagonalization.

At the first step, the total energy minimization is performed in order to find the equilibrium atomic structure of the crystal. For this purpose, we used CRYSTAL09 (Ref. 28) and VASP5.2 (Ref. 29) computer codes for checking abilities of both the LCAO and the PW approaches (see *ab initio* calculation details below). The calculated structure parameters were used for phonon calculations. One should notice that not every wave

vector k commensurates with any supercell. For a cubic STO, we used the $2 \times 2 \times 2$ supercell of 40 atoms since it is small enough to be calculated in a reasonable time but large enough to commensurate with four special k points of the BZ (Γ, R, X, M) of a simple cubic lattice. For the convenience of comparison, the same 40-atom supercell also was used for the AFD STO phase.

The calculation of forces induced by displaced atoms is the third step in phonon calculation. In practice, the weak point of the DFP method is the fact that the magnitude of atomic displacements is arbitrary in the force calculation, and the computer codes implementing this method could produce inconsistent results depending on a choice of this magnitude. Generally, the atomic displacements should not be too large to guarantee the linear relation between forces and displacements (as the harmonic approximation is used in DFP method). However, these displacements also should not be too small to avoid an effect of a numerical noise in the total energy second derivative calculation and, therefore, redundant calculation accuracy. Our experience shows that, for the STO crystal, the default value of the displacement magnitude of 0.003 Å in the CRYSTAL09 code is reasonable. However, the same magnitude in the VASP5.2 code seems to be insufficient as we obtained an anomaly of large acoustic phonon frequencies with this magnitude. The value of displacement magnitude in PW-based phonon calculations was fixed at 0.02 Å.

Thus, the forces obtained are collected in a dynamical matrix where the eigenvalues give squared phonon frequencies, and eigenvectors are equal to phonon modes. Unlike the VASP5.2 code, the CRYSTAL09 code allows for solving the dynamical matrix for all the symmetry k points commensurating with the supercell chosen. The VASP5.2 code permits calculating the frequencies only at the Γ point of the BZ independently of the supercell chosen (whereas, the classification of the calculated frequencies over other k points is additionally required).

In order to obtain the temperature dependence of the Helmholtz free energy F and heat capacity C_v, the integration over the phonon density of states is performed according to the equations,[30]

$$F = 3nNk_BT \int_0^{\omega_L} \ln \left\{ 2 \sinh \frac{\hbar\omega}{2k_BT} \right\} g(\omega)d\omega, \quad (1)$$

$$C_v = 3nNk_B \int_0^{\omega_L} \left(\frac{\hbar\omega}{2k_BT} \right)^2 \operatorname{csch}^2 \left(\frac{\hbar\omega}{2k_BT} \right) g(\omega)d\omega, \quad (2)$$

where n is the number of atoms per unit cell, N is the number of unit cells, ω_L is the maximum phonon frequency, and $g(\omega)\,d\omega$ is defined to be the fractional number of phonon frequencies in the range between ω and $\omega + d\omega$. Note that, within the harmonic approximation, the heat capacities taken at constant pressure and constant volume are equal ($C_v = C_p = C_{har}$) (Ref. 31). In our calculations, integration over the whole phonon spectrum is replaced by a summation over a finite number of frequencies defined by the size of the supercell used. As one can see, the phonon frequencies enter F, C_v through hyperbolic functions meaning—the lower the frequency, the greater its contribution. That is why one has to calculate the low-frequency (soft) phonon modes as accurately as possible,

TABLE II. Optimization of GTO outer exponents (bohr^{-2}).

Type	Nonoptimized	Optimized
	Sr (small core) $4s^2 4p^6 5s^2$	
$6s$	0.3344	0.3452
$5p$	0.7418	0.7296
$6p$	0.2801	0.2757
	Ti (small core) $3s^2 4p^6 3d^2 4s^2$	
$5s$	0.5128	0.6149
$5p$	0.3982	0.3426
$4d$	0.8002	0.7399
$5d$	0.2620	0.2936
	O (all electron) $1s^2 2s^2 2p^4$	
$3sp$	0.9057	0.8785
$4sp$	0.2556	0.2287
$3d$	1.2920	0.1480

in order to obtain the reasonable thermodynamic properties. One should also keep in mind that our DFP calculations neglect anharmonic effects, and this is why the obtained soft-mode frequencies and temperature dependencies of the Helmholtz free energy and heat capacity are not fully correct.

In the *ab initio* calculations of phonon properties using CRYSTAL09 (the LCAO basis set) and VASP5.2 (the PW basis set), we have chosen the DFT GGA-type PBE functional[32] and two hybrid [PBE0 (Ref. [33]) and B3PW (Ref. [34])] exchange-correlation functionals (currently B3PW is not implemented in VASP5.2). All these functionals have been successfully applied earlier for the calculations of bulk and surface perovskite properties.[14,20,35]

In all the LCAO calculations, the small-core relativistic effective core potentials (ECPs) for Ti and Sr atoms[36,37] were used, while the all-electron triple-ζ quality basis set for the O atom was taken from Ref. [38]. We follow a tradition of the CRYSTAL community, to use the same ECP in the calculations, irrespective of the exchange-correlation functional. Our ECPs are generated from HF calculations and constitute a reasonable choice [see Ref. [35] for more details].

It is well known that, in the LCAO calculations of crystals, the basis set of a free atom has to be modified as the diffuse outermost wave functions cause numerical problems because of the large overlap with the core functions of the neighboring atoms in a dense-packed crystal.[39] To optimize the basis set in the present paper, we used Powell's conjugate-directions minimization method[40] without calculations on the total-energy derivatives. It is known as one of the most efficient direct minimization methods. Being interfaced with the CRYSTAL09 code, our computer program OPTBAS (Ref. [41]) has been applied for the basis set optimization. The Gaussian-type orbital (GTO) exponents less than 0.1 bohr^{-2} were excluded, and the bound-constrained optimization was performed for the remaining exponents with 0.1 bohr^{-2} lower bound. The GTO exponents in noncontracted basis functions[36,37] were optimized in the PBE0 calculations for the cubic bulk STO and were compared with nonoptimized ones in Table II. One should note that the first attempt to optimize the LCAO basis set for STO has been performed only recently in the B3PW calculations.[35] One of the main differences between our basis set and that suggested in Ref. [35] is the use of the d-polarization

orbital on the Sr atom. In order to check its role, we also added a similar d orbital (0.4699 bohr^{-2}) (Ref. [35]) and optimized it (0.5029 bohr^{-2}) for our basis set. The results for these three basis sets (original atomic, optimized, and extended with one d orbital) are discussed and are compared below.

The following precision settings were applied in both CRYSTAL09 and VASP5.2 codes, unless otherwise stated. The Monkhorst-Pack[42] $8 \times 8 \times 8$ k-point mesh in the BZ was used. The tolerance of the energy convergence on the self-consistent field cycles was set to 10^{-10} a.u. and an extra-large pruned DFT integration grid was adopted. In the CRYSTAL09 code, the truncation criteria for bielectronic integrals (Coulomb and HF exchange series) were heightened [values 8, 8, 8, 8, 16 (Ref. [28])]. Additionally, the DFT density and grid weight tolerances were heightened [values 8 and 16 (Ref. [28])].

Within the PW framework, we used the projector augmented wave method[43] and the ECPs substituting for 28 core electrons on the Sr atom, 10 core electrons on the Ti atoms, and 2 core electrons on the O atoms. These ECPs were generated for the PBE functional. The plane-wave cutoff energy was fixed at 600 eV for both the geometry optimization and the phonon-frequency calculations. The electron occupancies in VASP5.2 were determined with the Gaussian method using a smearing parameter of 0.1 eV.

IV. RESULTS AND DISCUSSION

A. Cubic phase

The basic bulk properties of STO in a cubic phase, calculated using the LCAO and PW approaches as well as GGA-type PBE and hybrid PBE0 and B3PW functionals, are presented in Table III along with the experimental data. As one can see, the PBE functional in both the LCAO and the PW calculations considerably underestimates the band gap and overestimates the lattice constant. (This is a well-known trend in the GGA calculations, in general, and has been observed for STO, in particular, in Ref. [35].) Moreover, the band gap is more underestimated for the PW approach than in LCAO. The importance of the approach's proper choice is confirmed by a comparison of the LCAO results for the PBE0 functional with optimized and nonoptimized basis sets: The optimization improves agreement with the experiment not only for the band gap (electronic properties), but also for the crystal atomization energy and bulk modulus (thermochemical and mechanical properties). The addition of the Sr d-polarization orbital to the optimized basis set negligibly changes the bulk properties. The B3PW hybrid functional also gives very good results for most properties. Note that the results of PW PBE0 calculations are also close to the experimental data. However, the VASP calculations with the hybrid functionals are much more time consuming than similar CRYSTAL09 calculations. It is worth mentioning that the band gap in our calculations with the PBE0 functional is slightly overestimated in a comparison with the B3PW and experiment. Both LCAO and PW approaches combined with the PBE0 demonstrate this effect, which might be due to higher exact exchange contribution to the PBE0 functional. The same value of an exact exchange is also used in the HSE functional; however, the screening parameter may influence the band gap as discussed in Ref. [14].

TABLE III. Cubic STO basic properties.

| | | LCAO | | | | PW | | |
| | | PBE0 | | | | | | |
	PBE	Nonoptimized basis set	Optimized basis set	Optimized basis set + Sr$_d$	B3PW	PBE	PBE0	Experimental
Lattice constant a_0, Å	3.96	3.89	3.91	3.90	3.92	3.94	3.90	3.91 Ref. 44
Direct (and indirect) band gap, eV	2.1 (1.8)	4.3 (4.0)	4.2 (3.9)	4.2 (3.8)	3.7 (3.4)	2.1 (1.8)	4.4 (4.0)	3.8 (3.3) Ref. 45
Atomization energy, eV	31.6	28.5	29.3	30.0	29.1	32.8	32.2	31.7 Ref. 46
Bulk modulus, GPa	171	220	195	201	190	169	193	179 Ref. 47

The calculated TO and LO phonon frequencies for the cubic phase at the Γ and R points of the BZ are summarized in Tables IV and V. To calculate phonons in these points, the primitive unit cell should be doubled with the transformation matrix $\begin{pmatrix} 1 & 1 & 0 \\ 1 & 0 & 1 \\ 0 & 1 & 1 \end{pmatrix}$ of the lattice translation vectors.[39]

The upper and lower parts of Table IV present the results of phonon calculations for the Γ and R points, respectively. All the methods used predict the t_{1u} (TO1 mode) to be soft, in agreement with the experiments.[3,4] Its frequency is either imaginary or very low, depending on the particular functional. The B3PW functional suggests a much softer TO1 mode than PBE0. Moreover, in all PW calculations, it is imaginary. (It is important to be reminded that our calculations are performed in the harmonic approximation and, thus, are unable to correctly obtain the soft-mode frequencies.)

We observe instability for the calculated R_{4+} soft mode for the hybrid PBE0 functional, in agreement with the group-theoretical analysis (Sec. II) and inelastic neutron-

scattering experiments.[49] Depending on the inclusion of the d-polarization orbital on Sr ion in our optimized LCAO basis set, soft-mode frequency is either (relatively small) real or imaginary. Thus, this property is very sensitive to the choice of the LCAO basis set.

The basis set optimization in the LCAO approach greatly improves the results, in general, and reduces the relative errors for calculated frequencies by a factor of 2–5 with respect to the experimental data[49] (as compared with the nonoptimized basis set).

The PW calculations with the PBE0 functional also suggest high-quality results. Our results for the PW PBE0 calculations are very similar to those recently published for the HSE hybrid functional with screened Coulomb interactions.[14]

The results for high-frequency calculations are less sensitive to use the particular functional than those for low frequencies. There is a general trend for the hybrid functionals within the LCAO approach that the calculated phonon frequencies

TABLE IV. TO phonon frequencies (cm^{-1}) in cubic STO phase.

| | | | LCAO | | | | PW (This paper) | | PW (Ref. 14) | | Experimental (297 K) (Ref. 48),[a] (Ref. 49),[b] (Ref. 50)[b] |
		PBE	PBE0 nonoptimized basis set	PBE0 opt. basis set	PBE0 opt. basis set + Sr$_d$	B3PW	PBE	PBE0	PBE	HSE	
Γ	t_{1u} (TO1)	$71i$	63	72	69	17	$133i$	$100i$	$115i$	$74i$	42 (Ref. 48), 91 (Ref. 49)
	t_{1u} (TO2)	166	203	180	175	175	146	161	147	162	175 (Ref. 48), 170 (Ref. 49)
	t_{1u}	247	302	271	255	267	226	252	234	250	265 (Ref. 49)
	t_{1u} (TO3)	522	594	547	553	540	508	536	512	533	545(Ref. 48), 547 (Ref. 49)
R	R_{4+}	$16i$	92	70	$51i$	55	$86i$	$54i$	$\sim90i^c$	$\sim80i^c$	52 (Ref. 49)
	R_{5+}	144	177	153	144	149	128	138			145 (Ref. 49)
	R_{4-}	432	481	460	457	454	413	442			446 (Ref. 49)
	R_{5+}	437	493	465	451	461	419	449			450 (Ref. 49)
	R_{3+}	440	533	478	498	466	433	475			474 (Ref. 49)
	R_{1+}	804	906	861	872	848	798	857			~800 (Ref. 50)

[a]Infrared measurements.
[b]Inelastic neutron-scattering measurements.
[c]Taken from Fig. 3 in Ref. 14.

TABLE V. LO phonon frequencies (cm^{-1}) in cubic STO phase.

		LCAO				
		PBE0				
	PBE	Nonoptimized basis set	Optimized basis set	B3PW	PW LDA (Ref. 50)	Experimental (Ref. 48)
t_{1u} (LO1)	165	203	180	174	158	171
t_{1u} (LO2)	458	530	480	477	454	474
t_{1u} (LO3)	833	810	809	809	829	795

at the Γ and R points are slightly overestimated as compared with the experimental values ($\sim$10 cm^{-1} on average, except for the TO1 soft mode). On the contrary, the PW approach with PBE0 functional slightly underestimates ($\sim$7 cm^{-1}) phonon frequencies. On the other hand, the GGA functional within both the LCAO and the PW approaches considerably underestimates frequencies (on average, by $\sim$20 cm^{-1}).

The dependence of the soft-mode frequencies at the Γ and R points for the LCAO optimized basis sets with and without the d-polarization orbital on the Sr ion is plotted in Fig. 2 as a function of the lattice constant (which mimics thermal expansion of the lattice). As one can see, the soft mode at the R point increases very slowly, whereas, that at the Γ point decreases considerably, supporting the idea[5] about their concurrent character. The optimized basis set with the d orbital on the Sr atom (gray curves) demonstrated imaginary frequencies for the R_{4+} mode at all lattice parameter values considered. The recent simulations using the ABINIT code with the GGA-type PW91 functional[18] and HSE hybrid functional[14] have shown the same trend at the R point.

The agreement with the experiment for three LO frequencies (Table V) is also very good as well as the magnitude of the LO-TO splitting.[51] The earlier PW calculations within the standard LDA approximation[5] gave worse results than our hybrid-functional calculations.

B. Tetragonal AFD phase

The basic structural properties for the tetragonal AFD phase are presented in Table VI for the LCAO with three different functionals and for the PW with the PBE functional

(we were unable to perform PW calculations with hybrid functionals as they are extremely time consuming). Along with the two lattice constants a ($= b$) and c, the O-ion position parameter u and the relevant TiO_6-octahedra rotation angle are compared. First, the LCAO calculations with the hybrid PBE0 functional and optimized basis set give the best agreement with the experiment. Second, despite the results of the PBE for different pseudopotentials and approaches (CRYSTAL09 and VASP5.2 codes) for a cubic phase being quite similar (Table III), they *differ* for the AFD phase (Table VI). For example, the octahedra rotation angle is well reproduced by the LCAO approach but is strongly overestimated by the PW. (Moreover, the rotation angle is obtained almost the same in LCAO calculations with different functionals). Obviously, this is not an effect of different pseudopotentials but of the two different approaches. We attribute this to the problems of reproducing tiny structure modifications using the PW approach (see also Refs. 5 and 14).

We analyzed cubic and tetragonal phase energies in detail in Table VII. Two hybrid functionals, B3PW and PBE0, give moderate total electronic energy gain ΔE for the tetragonal AFD phase with respect to the cubic one, whereas, for the PBE, this gain is only 0.6 meV. It is also necessary to take the zero-point vibration energies ΔE_{ZP} (second row) into account, which results in a small AFD final energy gain (not exceeding 20 meV) for all the functionals used within the LCAO scheme. Calculating the zero-point energies, we compared the values for the cubic and tetragonal AFD supercells with the *same* number of atoms. The temperature dependence of the Helmholtz free energies based on frequencies will be discussed below.

TABLE VI. AFD STO structural properties.

	LCAO			PW	
	PBE	PBE0 optimized basis set	B3PW	PBE	Experimental
Lattice constants, Å a	5.594	5.532	5.545	5.566	5.507 [50 K (Ref. 24)]
c	7.922	7.831	7.854	7.908	7.796 [50 K (Ref. 24)]
Cubic-tetragonal distortion $c/(\sqrt{2}a)$	1.0014	1.0011	1.0014	1.0046	1.0010 [50 K (Ref. 24)]
					1.0006 [65−110 K (Ref. 25)]
O-atom position, u, fractional un.	0.245	0.246	0.245	0.228	0.240 [4 K (Ref. 4)]
					0.241 [50 K (Ref. 24)]
					0.244 [77 K (Ref. 4)]
TiO_6-rotation angle arctan $(1 - 4u)$,°	1.1	0.9	1.1	4.9	2.1 [4 K (Ref. 4)]
					2.0 [50 K (Ref. 24)]
					1.4 [77 K (Ref. 4)]
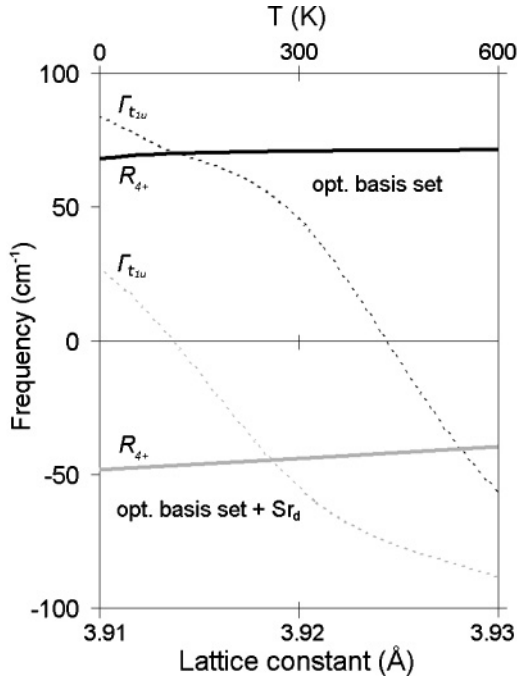
FIG. 2. Γ and R soft phonon modes vs temperature dependence calculated via PBE0 (upper and lower parts correspond to the LCAO basis set with and without the Sr d-polarization orbital). Imaginary frequencies are represented by negative values.

Lastly, the phonon frequencies for the AFD phase are presented in Table VIII where the theoretical predictions for Raman, infrared, and silent modes are compared with the experimental data and theoretical PW calculations[5] within the LDA-type functional (performed only for the infrared phonons). As before, the hybrid functionals within the LCAO approach tend to overestimate the phonon frequencies compared with the experimental values, whereas, the GGA functional (combined within both the LCAO and PW approaches) tends to underestimate frequencies.

The main conclusions are the following. (i) The PBE0 functional with the optimized basis set gives the best agreement with the experimental data (when available). (ii) The splitting of three infrared cubic t_{1u} modes (denoted by curly brackets in Table VIII) is predicted to be small, 2, 4, and 11 cm^{-1}. (iii) Several soft modes are found, indicating a possible instability of the tetragonal AFD phase at the temperatures close to 0 K as discussed in Ref. 5.

C. Heat capacity and Helmholtz free energy

The temperature dependence of heat capacity has been calculated using Eq. (2) for both STO phases using the PBE,

TABLE VII. Total electronic energy difference ΔE and zero-point energy difference ΔE_{ZP} (meV per unit cell) of cubic and tetragonal AFD STO phases with respect to the cubic phase, calculated via the LCAO method.

	PBE	PBE0 optimized basis set	B3PW
ΔE	−0.6	−2.9	−1.8
ΔE_{ZP}	−12.4	−16.7	−14.5
Total	−13.0	−19.6	−16.3
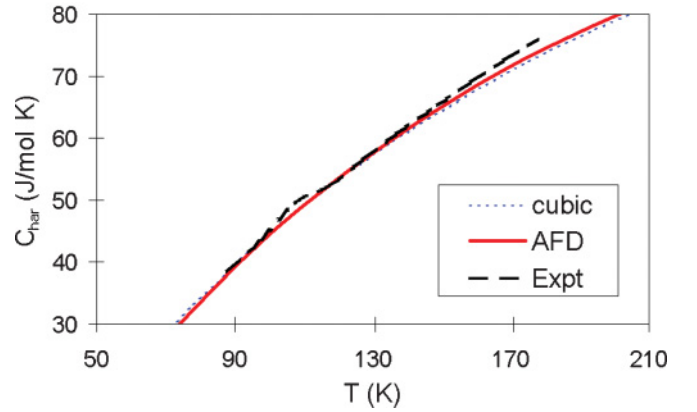
FIG. 3. (Color online) Heat capacity calculated using the PBE0 functional (and optimized LCAO basis set).

PBE0, and B3PW functionals (only the results for the second one is shown in Fig. 3). In all three cases, the agreement with experiment[53] is very good; in a wide temperature range, the calculated curves lie very close to the experimental line. The only heat-capacity calculations[19] were performed so far for the STO cubic phase using the all-electron linear augmented plane-wave method (WIEN-2K code); the results are very close to our calculations.

Using the CRYSTAL09 code, we also calculated the Helmholtz free energy for the PBE0 functional [Eq. (1)] as the function of the temperature. As the temperature rises from 0 to 300 K, the free energies for both phases decrease by ~0.2 eV/cell. In the whole temperature range, the energy curve for the AFD phase lies slightly below (~20 meV) that for the cubic phase. This contradicts the experimental fact that these curves cross at the phase-transition temperature. We assume that this contradiction occurs due to the use of the harmonic approximation and a discrete phonon spectrum in Eq. (1). As a result, our calculation accuracy becomes comparable with mentioned energy differences for the two phases.

V. CONCLUSIONS

The group-theoretical analysis of the phonon symmetry indicates that the observed AFD phase transition is caused by softening of the R_{4+} phonon mode; no other modes are necessary. This is in complete agreement with our calculations. We also performed a classification of the calculated frequencies into the Raman, infrared, and silent modes.

The use of the *hybrid* PBE0 functional in the framework of both approaches, LCAO and PW, gives better phonon frequencies compared to the GGA-type functionals. Another advantage of the hybrid functionals is a better reproduced band gap in comparison to the experiments, in contrast to its strong underestimation while using the GGA functionals (see also Ref. 54). Furthermore, with the use of hybrid functionals, no explicit preference for the LCAO or PW approach in the phonon calculations could be given. One should note that the hybrid DFT LCAO calculations in CRYSTAL09 are much faster compared with the extremely time-consuming hybrid DFT PW calculations in VASP5.2. On the other hand, a comparison of the phonon frequencies and atomic structure of the cubic

TABLE VIII. Phonon frequencies (cm^{-1}) in the AFD STO phase.

			LCAO					
				PBE0				
		PBE	Nonoptimized basis set	Optimized basis set	B3PW	PW PBE	PW LDA (Ref. 5)	Experimental (15 K)
Raman	a_{1g}	29	78	63	61	98		48 (Ref. 50)
	e_g	48	99	79	76	*17i*		15 (Ref. 50)
	e_g	137	168	146	144	183		143 (Ref. 50)
	b_{2g}	152	181	158	157	140		[235 (Ref. 50)]
	b_{2g}	441	534	466	462	421		
	e_g	444	537	468	465	425		460 (Ref. 50)
	b_{1g}	438	501	479	469	437		
Silent	a_{2g}	440	502	480	470	434		
	a_{2g}	806	908	862	850	793		
	b_{1u}	252	308	275	271	245		
	a_{1u}	430	478	458	452	410		
Infrared	a_{2u}	2	101	68	28⎫	*4i*	*90i*	
	e_u	1	103	72	45⎭	*28i*	*96i*	
	e_u	163	199	177	174⎫	183		
	a_{2u}	180	211	189	187⎭	158	157	185 (Ref. 52)
	e_u	252	306	273	270	239	240	
	e_u	433	481	460	455	411	419	450 (Ref. 52)
	e_u	523	597	549	542⎫	504	515	
	a_{2u}	526	599	551	544⎭	510		

and tetragonal AFD STO phases calculated within the LCAO approach using optimized and nonoptimized basis sets clearly demonstrates that the basis set optimization gives much better results. We have also shown that the Sr *d*-polarization orbital used in the LCAO basis set significantly affects the calculated soft-mode frequencies.

The detailed calculations of phonon frequencies in the tetragonal phase have been performed. The splitting of the phonon frequencies $t_{1u} \rightarrow a_{2u} + e_u$ due to the AFD phase transition is predicted to be rather small, 2–11 cm^{-1}. Lastly, the experimental temperature dependence of the STO heat capacity is successfully reproduced.

Based on this experience for defect-free STO, we plan to use the LCAO approach combined with the hybrid functionals for further thermodynamic study of defective perovskites under finite temperatures. This is important for the prediction of the material properties and device performance (e.g., sensors and solid oxide fuel cells) under realistic operational conditions.

[1]H.-J. Donnerberg, *Atomic Simulations of Electro-Optical and Magneto-Optical Materials*, Springer Tracts in Modern Physics (Springer, Berlin, 1999), Vol. 151.

[2]R. Merkle and J. Maier, Angew. Chem. **47**, 3874 (2008).

[3]M. E. Lines and A. M. Glass, *Principles and Applications of Ferroelectrics and Related Materials* (Clarendons, Oxford, 1977).

[4]H. Unoki and T. Sakudo, J. Phys. Soc. Jpn. **23**, 546 (1967).

[5]N. Sai and D. Vanderbilt, Phys. Rev. B **62**, 13942 (2000).

[6]J. F. Scott, Rev. Mod. Phys. **46**, 83 (1974).

[7]K. A. Müller, W. Berlinger, and E. Tosatti, Z. Phys. B **84**, 277 (1991).

[8]A. K. Tagantsev, E. Courtens, and L. Arzel, Phys. Rev. B **64**, 224107 (2001).

[9]V. V. Lemanov, Ferroelectrics **265**, 1 (2002).

[10]O. E. Kvyatkovskii, Phys. Solid State **43**, 1345 (2001).

[11]C. LaSota, C. Wang, R. Yu, and H. Krakauer, Ferroelectrics **194**, 109 (1997).

[12]K. Parlinski, Z. Q. Li, and Y. Kawazoe, Phys. Rev. Lett. **78**, 4063 (1997).

[13]S. Baroni, P. Giannozzi, and A. Testa, Phys. Rev. Lett. **58**, 1861 (1987).

[14]R. Wahl, D. Vogtenhuber, and G. Kresse, Phys. Rev. B **78**, 104116 (2008).

[15]A. Lebedev, Phys. Solid State **51**, 362 (2009).

[16]T. Trautmann and C. Falter, J. Phys. Condens. Matter **16**, 5955 (2004).

[17]N. Choudhury, E. J. Walter, A. I. Kolesnikov, and C.-K. Loong, Phys. Rev. B **77**, 134111 (2008).

[18] Y. Xie, H. Yu, G. Zhang, and H. Fu, J. Phys. Condens. Matter **20**, 215215 (2008).

[19] A. Boudali, M. D. Khodja, B. Amrani, D. Bourbie, K. Amara, and A. Abada, Phys. Lett. A **373**, 879 (2009).

[20] E. Heifets, E. A. Kotomin, and V. Trepakov, J. Phys. Condens. Matter **18**, 4845 (2006).

[21] R. A. Evarestov and V. P. Smirnov, *Site Symmetry in Crystals: Theory and Applications*, Springer Series in Solid State Sciences (Springer, Berlin, 1993), Vol. 108.

[22] Bilbao Crystallographic Web-Server [http://www.cryst.ehu.es].

[23] A. Cracknell, B. Davies, S. Miller, and V. Love, *Kronecker Product Tables*, I General Introduction and Tables of Irreducible Representations of Space Groups (IFI/Plenum, New York, Washington-London, 1979).

[24] W. Jauch and A. Palmer, Phys. Rev. B **60**, 2961 (1999).

[25] W. Lytle, J. Appl. Phys. **35**, 2212 (1964).

[26] C. J. Howard and H. T. Stokes, Acta Crystallogr., Sect. A: Found. Crystallogr. **61**, 93 (2005).

[27] R. A. Evarestov and M. V. Losev, J. Comput. Chem. **30**, 2645 (2009).

[28] R. Dovesi, V. R. Saunders, C. Roetti, R. Orlando, C. M. Zicovich-Wilson, F. Pascale, B. Civalleri, K. Doll, N. M. Harrison, I. J. Bush, P. D'Arco, and M. Llunell, *CRYSTAL09 User's Manual* (University of Torino, Italy, 2008).

[29] G. Kresse and J. Hafner, *VASP the Guide* (University of Vienna, 2007) [http://cms.mpi.univie.ac.at/vasp/]; G. Kresse and J. Furthmüller, Comput. Mater. Sci. **6**, 15 (1996); G. Kresse and J. Hafner, Phys. Rev. B **47**, RC558 (1993); G. Kresse and J. Furthmüller, Phys. Rev. B **54**, 11169 (1996).

[30] C. Lee and X. Gonze, Phys. Rev. B **51**, 8610 (1995).

[31] G. Grimvall, *Thermophysical Properties of Materials* (Elsevier, New York, 1999).

[32] J. P. Perdew, K. Burke, and M. Ernzerhof, Phys. Rev. Lett. **77**, 3865 (1996).

[33] M. Ernzerhof and G. E. Scuseria, J. Chem. Phys. **110**, 5029 (1999).

[34] A. D. Becke, J. Chem. Phys. **98**, 5648 (1993).

[35] S. Piskunov, E. Heifets, R. I. Eglitis, and G. Borstel, Comput. Mater. Sci. **29**, 165 (2004); S. Piskunov, E. A. Kotomin, E. Heifets, R. I. Eglitis, and G. Borstel, Surf. Sci. **575**, 75 (2005).

[36] M. M. Hurley, L. F. Pacios, P. A. Christiansen, R. B. Ross, and W. C. Ermler, Chem. Phys. **84**, 6840 (1986).

[37] L. A. LaJohn, P. A. Christiansen, R. B. Ross, T. Atashroo, and W. C. Ermler, J. Chem. Phys. **87**, 2812 (1987).

[38] A. Schäfer, C. Huber, and R. Ahlrichs, J. Chem. Phys. **100**, 5829 (1994).

[39] R. A. Evarestov, *Quantum Chemistry of Solids. The LCAO First Principles Treatment of Crystals,* Springer Series in Solid State Sciences (Springer, Heidelberg, 2007), Vol. 153.

[40] W. H. Press, S. A. Teukolsky, V. T. Vetterling, and B. P. Flannery, *Numerical Recipes in FORTRAN 77*: The Art of Scientific Computing (Press Syndicate of the University of Cambridge, New York, 2001).

[41] R. A. Evarestov, A. I. Panin, A. V. Bandura, and M. V. Losev, J. Phys.: Conf. Ser. **117**, 012015 (2008).

[42] H. J. Monkhorst and J. D. Pack, Phys. Rev. B **13**, 5188 (1976).

[43] P. E. Blöchl, Phys. Rev. B **50**, 17953 (1994).

[44] L. Cao and E. Sozontov, and J. Zegenhagen, Phys. Status Solidi A **181**, 387 (2000).

[45] K. Van Benthem, C. Elsaesser, and R. H. French, J. Appl. Phys. **90**, 6156 (2001).

[46] D. Ricci, G. Bano, G. Pacchioni, and F. Illas, Phys. Rev. B **68**, 224105 (2003).

[47] *Ferroelectrics and Related Substances,* edited by K. H. Hellwege and A. M. Hellwege, Landolt-Börnstein, New Series, Group III (Springer-Verlag, Berlin, 1969), Vol. 3.

[48] J. L. Servoin, Y. Luspin, and F. Gervais, Phys. Rev. B **22**, 5501 (1980).

[49] W. G. Stirling, J. Phys. C **5**, 2711 (1972).

[50] P. A. Fleury, J. F. Scott, and J. M. Worlock, Phys. Rev. Lett. **21**, 16 (1968).

[51] W. Zhong, R. D. King-Smith, and D. Vanderbilt, Phys. Rev. Lett. **72**, 3618 (1994).

[52] J. C. Galzerani and R. S. Katiyar, Solid State Commun. **41**, 515 (1982).

[53] I. Hatta, Y. Shiroishi, K. A. Müller, and W. Berlinger, Phys. Rev. B **16**, 1138 (1977).

[54] D. I. Bilc, R. Orlando, R. Shaltaf, G. M. Rignanese, J. Iniguez, and P. Ghosez, Phys. Rev. B **77**, 165107 (2008).